

Nonlinear optical frequency conversion applied to remote sensing receiver systems

P. E. Powers^(a), S. Sriram^(b), and S. A. Kingsley^(b)

^aDepartment of Physics and the Electro-Optics Program, University of Dayton
300 College Park, Dayton OH 45469-2314

^bSrico, Inc. 2724 Sawbury Blvd, Columbus, OH 43235-4579

Abstract

We present results of a receiver system based on frequency converting mid-infrared wavelengths to the 1.5 μm region using periodically-poled lithium niobate (PPLN). By doing so optical amplifiers and avalanche photodetectors (APDs) developed for the fiber optics communications industry can be used, thus providing very high detection sensitivity and high speed without the need for cryogenically cooled mid-infrared detectors. Laboratory experiments using APD detection for 3 μm , 2.5 nsec FWHM pulses that have been frequency converted to 1.5 μm demonstrate detection sensitivities as low as 1.5×10^{-13} Joules.

1. Introduction

Remote sensing systems, such as Light Detection and Ranging (LIDAR), have benefited greatly from nonlinear sources capable of generating tunable mid-infrared wavelengths (3-5 microns). Much work has focused on increasing the energy output of these sources so as to improve the system's range. We present an approach that improves the range of a LIDAR system by employing nonlinear optical techniques in the receiver.

Detection in the 3 to 5 μm region has traditionally made use of liquid nitrogen cooled detectors but more recently newer thermo-electrically (TE) cooled detectors have become available. The TE-cooled detectors are the most convenient to work with and can have a low noise equivalent power (NEP). For applications such as LIDAR high speed can be important and these detectors have a higher NEP than slower detectors. Sensitivity comparisons between state-of-the-art detectors (both cryogenic and TE cooled) HgCdTe, HgCdZnTe and InSb show that their NEP are between 0.1 to 10 nW/ $\sqrt{\text{Hz}}$. For example, the NEP of a commercially available TE cooled HgCdZnTe detector with a time constant of 125 nsec is 4 nW/ $\sqrt{\text{Hz}}$.¹ The bandwidth of this detector is 8 MHz so that an energy of 1.4 pJ in a 125 nsec time interval would lead to an SNR of 1.

An alternative to detection in the 3 to 5 μm range is to frequency convert the return signal to the near IR or to the visible.^{2, 3, 4, 5} The advantage of this scheme is that much higher sensitivity detectors may be used, including photon counting detectors. Detection technology in the near IR and visible is a much more mature technology than the mid IR and detection systems can take advantage of well developed telecommunications technology. Detectors in the near IR and visible can have a low NEP and have high speed. For example, the InGaAs APD used in this work is capable of detecting 1.8×10^{-5} pJ in a 6 nsec pulse. To compare with the slower mid-IR detector presented above, this corresponds to being able to detect 3.8×10^{-4} pJ in a 125 nsec time interval with an SNR of 1. Because of the much higher sensitivity, low efficiency frequency conversion processes can be considered as part of a viable detection scheme. The combination

of frequency conversion to the visible or NIR with high sensitivity detectors results in an overall NEP similar to or better than direct detection in the IR, but with a much higher response time.

With the upconversion scheme, one must decide on a target upconverted wavelength. In this work we chose to focus on converting to 1.55 μm so as to take advantage of well developed telecommunications detectors and systems. The upconversion process can occur in several forms. We will consider only upconversion schemes based on nonlinear optical $\chi^{(2)}$ processes. A true upconverter scheme would take the return photon and sum it with that of a reference “pump” laser. To convert from the 3 to 5 μm to the telecom wavelengths (roughly 1.55 μm) requires a pump laser with a wavelength between 2 and 3 μm . Lasers in this wavelength range are not as commonly available as, for example, a Nd:YAG laser. As sources in this wavelength range are further developed, they would provide a practical means of upconversion. The other approach is difference frequency generation between a pump laser and the 3 to 5 μm return generating a NIR 1.55 μm signal. The advantage of this technique is that the commonly available Nd:YAG laser operating at 1.064 μm results in a DFG signal near 1.55 μm . This is the technique we employ and we describe it more fully in the following sections.

A final consideration for the conversion process is to come up with a scheme to convert a given pulsed return whenever it arrives. Ideally a high peak power pulsed laser could be used as the pump laser for these conversion processes, but this requires that the pump laser to be synchronized with the return. If such knowledge is available then this would be the best approach. However, for applications such as LIDAR where the pulsed return signal may depend on varying ranges then the conversion process must be able to work no matter when the pulse returns. The strategy we have taken is to use a high power continuous wave (cw) laser as the pump. This combined with the high sensitivity of NIR and visible detectors can result in detection efficiencies better than direct mid-IR detectors while providing much higher response times.

2. Optical Frequency Converter

In order to avoid confusion with traditional terminology, we use the following expressions for the interacting waves in the frequency conversion process: the pump is the highest energy photon, the LIDAR return is the lowest energy photon, and the DFG photon will be called the signal. With this terminology, the difference frequency process is given by the following energy conservation equation:

$$\omega_{\text{DFG}} = \omega_{\text{p}} - \omega_{\text{return}}$$

This process can also be thought of as optical parametric amplification of the LIDAR return. The amplification comes about because in the DFG process the pump photons split into two photons of lesser energy (dictated by phase matching). This means that every time a pump photon splits into a DFG photon, a corresponding photon at the return wavelength is also generated. In this experiment the amplified LIDAR return rejected and the DFG signal is detected instead.

While several methods of phase matching are possible, by far the most effective approach involves quasi-phase-matching using a periodically poled ferroelectric material such as LiNbO₃ (PPLN). Quasi-phase-matching (QPM) has many advantages over other techniques. Unlike the case in birefringent phase matching, the largest second-order coefficient in the material is used and spatial walk-off is avoided. Thus, phase matching can be maintained over very long lengths.

The higher second-order coefficient in lithium niobate and the quasi-phase-matching results in much higher conversion efficiencies. These are important considerations when using a cw laser as the pump. Perhaps the greatest advantage is that the QPM process is easy to engineer. By appropriately choosing the grating period Λ , any nonlinear interaction between waves of any wavelength within the transparency band of the material can be quasi-phase matched.

An important issue to consider with the frequency conversion approach is the acceptance angle over which the frequency conversion is efficient. This acceptance angle is dictated by phasematching. In this work we do not yet address this issue, but point to other work such as that by Brewer et al who demonstrated image upconversion using a multi-lens array to overcome the acceptance angle issues.^{4, 5, 6}

The experimental setup is shown in Figure 1. 3 μm pulses of light to simulate the LIDAR returns were generated from a seeded optical parametric generator (OPG).^{7,8} The output energy of the OPG was on the order of 10 μJ and was attenuated with calibrated neutral density filters. The pump for the frequency conversion stage is a Light Solutions CW laser that generates 4.4 W. A cw source is used to enable us to eliminate timing issues with the LIDAR return. This pump is focused into the PPLN crystal with a 15 cm focal length lens. The cw pump beam size was 170 μm ($1/e^2$ intensity diameter). The pump beam and the LIDAR return beam were aligned such that they overlap in the crystal. At the output of the crystal, the 1.064 μm pump beam is rejected and the 1.5 μm signal beam is transmitted. The band-pass filter (BPF) blocks the 3-5 μm idler photons. The 1.5 μm signal beam is collimated with a 15 cm focal length lens and then coupled into a single mode fiber and the APD receiver. The single mode fiber was used because it was directly coupled to the APD detector. Better coupling efficiency could be obtained using a multimode fiber connected to the APD.

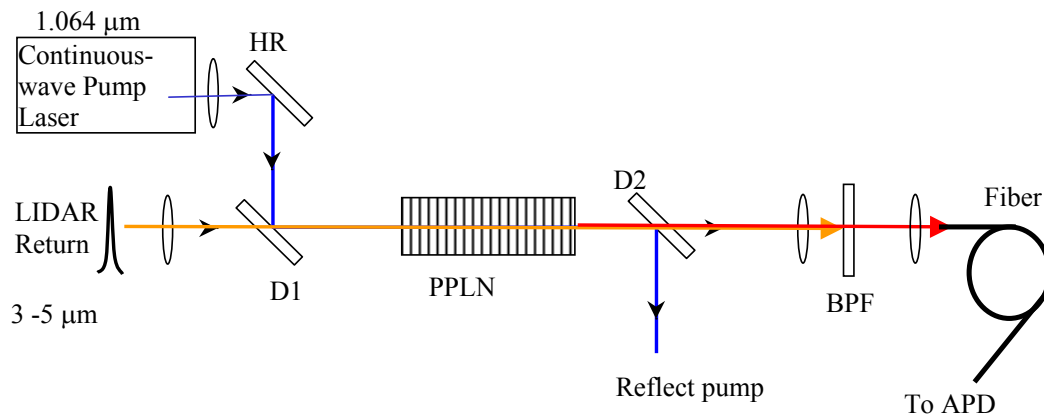


Figure 1. Setup to generate telecom wavelengths from the LIDAR return at 3 to 5 μm . PPLN pitch is 29.75 microns, LIDAR wavelength is 3.36 microns, up-converted wavelength is 1.557 microns. D1: dichroic mirror that combines the pump with the LIDAR return, D2: dichroic that reflects the pump and transmits 1.55 μm , BPF: filter passes 1.55 μm while blocking LIDAR wavelength.

3. High Sensitivity InGaAs Avalanche Photodiode (APD)

To demonstrate that the overall sensitivity of a LIDAR system employing a PPLN wavelength converter was superior to that of a system employing direct detection at 3 microns, a very sensitive optical receiver was designed and constructed for operation at 1.5 microns. The bandwidth of the APD receiver was designed to be about 1 MHz to 2.5 GHz when terminated in 50Ω . The high bandwidth APD chosen for this receiver was the Fujitsu FRM5W232BS⁹ device that was designed for digital applications. It has a single mode fiber pigtail and is contained in a mini-DIL package. The device also includes an amplifier with a high transimpedance of $2.2 \text{ k}\Omega$. It was selected on the basis of having one of the highest digital sensitivities (-33 dBm) among the few commercial products available. The APD has complementary outputs, but only the non-inverting output was used. The unused output was internally connected using a 50Ω surface mount termination.

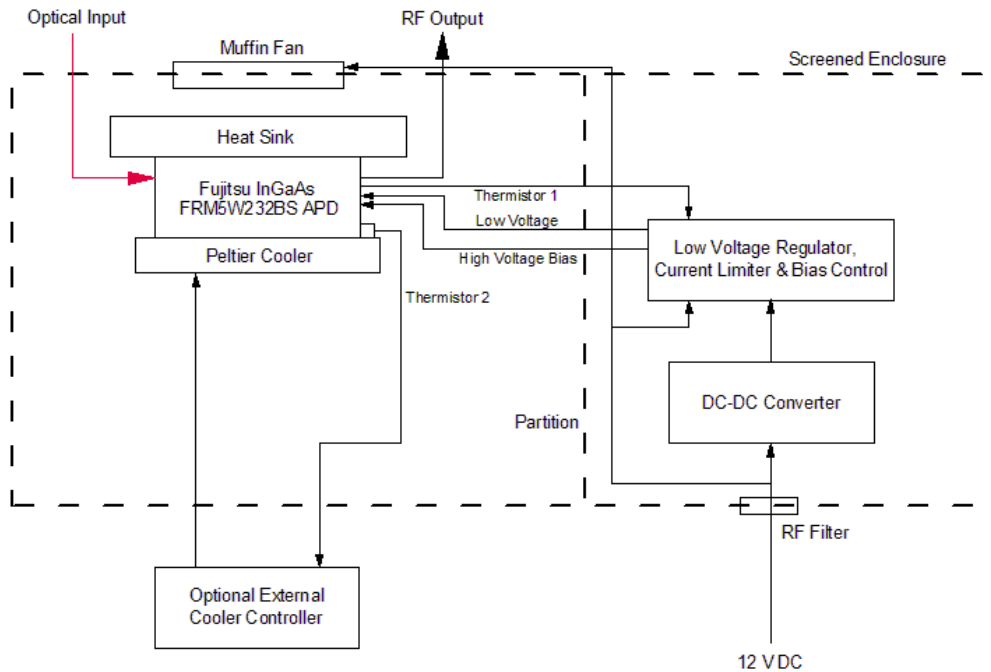


Figure 2. InGaAs APD receiver block diagram

Figure 2 shows the block diagram of the APD receiver. A control circuit stabilizes the gain against variations in temperature, limits the peak current to safe levels and prevents the APD from accidental forward bias. The APD package contains a thermistor for use with the bias control circuitry. A separate thermistor, mounted outside but close to the package, is used for controlling the temperature of a two-stage fan-assisted TE cooler.

The TE cooler maintains the APD at a constant temperature that stabilizes the gain. The APD dark current may be reduced by cooling the device and thus improve the receiver sensitivity. A reduction in the operating temperature of 25 C reduces the dark current by a factor of about 10. This APD temperature differential requires a sustained TE cooler current of about 1.5 A .

The gain versus bias voltage characteristics was obtained for the APD receiver at a wavelength of $1.55 \mu\text{m}$. This was done for several operating temperatures and input optical powers. The calibration data are required to characterize the performance of the frequency conversion

process. For calibration purposes a square-wave intensity modulated optical signal at 100% modulation was input into the APD receiver. This calibration was done at 3 MHz with an effective load of 1 MΩ. This avoids signal differentiation effects since the low frequency cut-off falls to about 70 kHz when the receiver is terminated in 1 MΩ. The peak power of the square-wave intensity modulated optical signal was 3 dB above its mean value. This mean value was measured using a standard hand-held optical power meter. Thus it was possible to determine the peak power applied to the APD receiver. Because this particular APD contained an automatic gain control (AGC) block, measurements were undertaken to ascertain that the response to 50% duty-cycle 3 MHz square-waves was the same as for low duty cycle pulses. Results indicated that the APD response was independent of duty cycle, and that the AGC function was proportional to the peak pulse amplitude – not its duration.

Figure 3 shows how the APD receiver responsivity into a 50 Ω load changes with bias voltage at an operating temperature of 10 C. These curves were later used to convert the digital sampling oscilloscope (DSO) displayed pulse amplitude into received energy at 1.55 μm. Detected optical power was converted to energy by multiplying the peak optical power by the 2.5 ns Full Width Half Maximum (FWHM) pulse width, so that a peak power of 100 nW was equivalent to a pulse energy of 2.5 x 10⁻¹⁶ J.

Using the Figure 3 transfer curve for a bias voltage of 49.0 V, a pulse of about 2.5 x 10⁻¹⁶ J (100 nW) produces a peak output voltage into a 50 Ω load of about 1 mV. To measure these small voltages with the DSO, a 20 dB amplifier was used to increase the amplitude by a factor of ten.

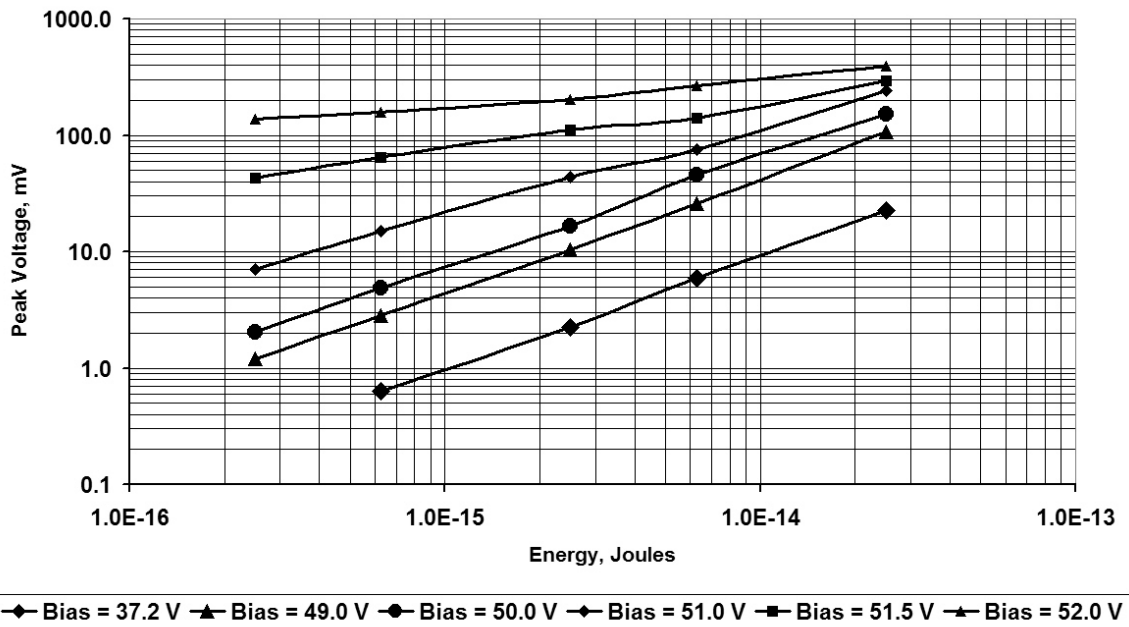


Figure 3. Calibration voltage responsivity curves for the Fujitsu FRM5W232BS InGaAs APD at 10 C with 50 Ω termination. Pulse width is assumed to be 2.5 ns.

4. PPLN Frequency Converter Performance with 1.5 micron APD Receiver

A DSO is used to measure and compare the frequency converted 1.55 micron output signal to the 3 μm input. The OPG source used to generate the 3 μm return introduced electromagnetic interference due to Q-switching. A 50 m fiber optic delay line was used before the APD receiver to provide a delay to the optical beam. As a result the electrical signal produced by the APD reaches the DSO long after the electromagnetic radiation due to the Q-switching of the laser. High-grade coaxial cables were employed to connect the APD Receiver to the post-detection amplifier and the latter to the DSO. This significantly reduced interference pick-up from the Q-switched laser.

Figure 4 shows the PPLN converter response for a strong 3 μm signal (4.3×10^{-10} J). The FWHM of the 1.5 μm up-converted pulse (6.5×10^{-14} J) in Figure 4 is about 3 ns. Figure 5 shows the 1.5 micron up-converted APD signal for a very weak LIDAR signal, near the system noise floor. The signal was averaged over 20 scans. This signal was produced by a 3 micron pulse at an energy level of 1.51×10^{-13} J and the corresponding 1.5 micron pulse was at an energy level of 3×10^{-17} J.

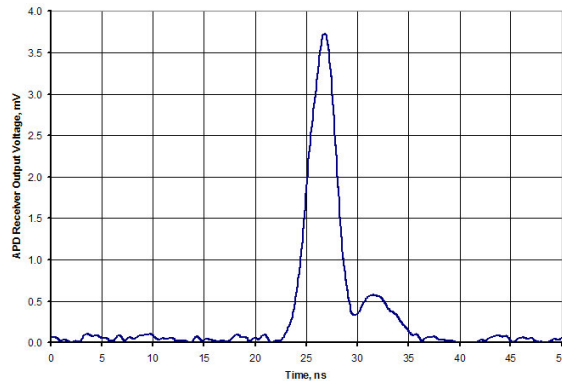


Figure 4. PPLN converter response for a strong 3 μm signal. APD bias voltage = 32.7 V, temperature = 10 C. Pump power = 4.4 W. Pulse energy at 3 μm = 4.3×10^{-10} Joules. Pulse energy at 1.5 μm = 6.5×10^{-14} Joules.

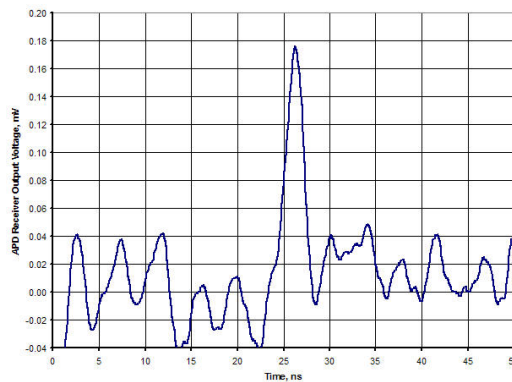


Figure 5. Received PPLN wavelength converter signal at the noise floor of the system after integration 20 times. APD bias voltage = 51.0 V, at a temperature of 10 C. The pump power was 4.4 W. The input pulse energy at 3 μm = 1.51×10^{-13} Joules, while the wavelength converted pulse energy at 1.5 μm = 5×10^{-17} Joules.

Figure 6 shows the ideal and measured performance of the PPLN wavelength converter. The ideal case assumes a Gaussian spatial and temporal beam profile and was calculated using the nonlinear optical modeling software, SNLO.¹⁰ The peak intensity at the converted wavelength of 1.55 μm was determined using the calibrated APD receiver. The minimum detectable energy at 1.55 μm was about 5×10^{-17} Joules. This corresponded to an input energy at 3 μm of about 1.5×10^{-13} Joules, equivalent to about 4 nW/ $\sqrt{\text{Hz}}$. The difference between the measured and ideal values is attributed to a non-ideal case that assumed a lossless system, a perfect non-linear crystal, Gaussian spatial and temporal beam profiles and a single longitudinal mode pump. However, the measured values follow the predicted trendline shown in the figure.

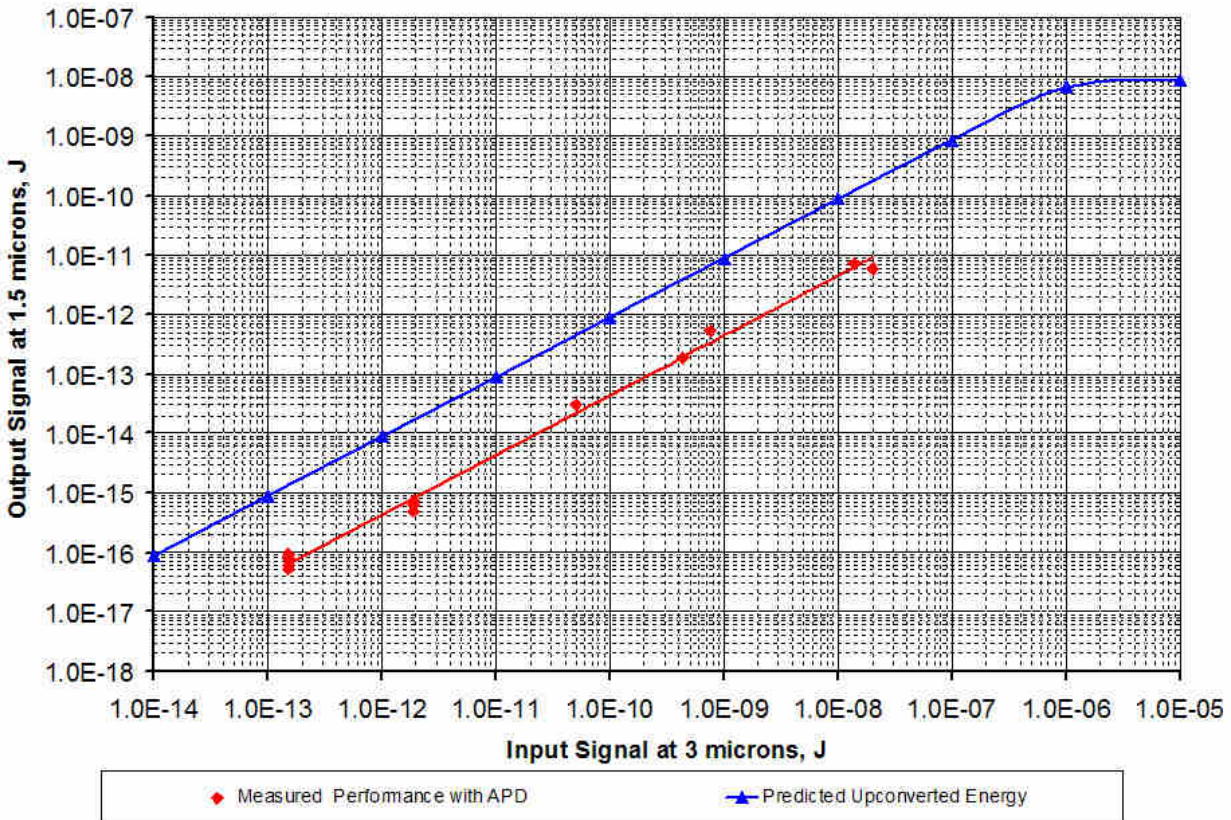


Figure 6. The performance of the PPLN wavelength converter. The pump signal was at a wavelength of 1.064 μm with a FWHM beam diameter of 300 μm and a power of 4.4 W. The Idler was at a wavelength of 3.3 μm with a FWHM beam diameter of 550 μm .

5. Conclusion

To conclude, we show Table 1 which compares the performance achieved by the PPLN converter to that of commercially available IR detectors. Sensitivity comparisons between state-of-the-art HgCdTe, HgCdZnTe and InSb detectors show that their Noise Equivalent Power (NEP) are between 10^2 to 10^4 pW/ $\sqrt{\text{Hz}}$. The measured NEP for our frequency converter was about 10^3 pW/ $\sqrt{\text{Hz}}$. This puts our measured results for the near room-temperature prototype converter on par with conventional technology based on cryogenically-cooled detectors. However, while the conventional detectors have bandwidths between 10 kHz and 10 MHz, the wavelength converter is essentially unlimited (2.5 GHz for the prototype), allowing for very high

range resolution, if needed. By further optimizing the system, the NEP can theoretically be reduced to approximately $1 \text{ pW}/\sqrt{\text{Hz}}$.

Table 1: LIDAR Optical Receiver Sensitivity Comparisons

Optical Receiver	Vendor	Model	Dimensions	Time-Constant	Bandwidth	Temp. K	D* (cm. $\sqrt{\text{Hz.W}}$)	NEP (pW/ $\sqrt{\text{Hz}}$)
PPLN Wavelength Converter	SRICO	NA	NA	NA	2.5 GHz	283	NA	
Predicted					250 MHz			1.8×10^2
Measured					250 MHz			3.8×10^3
Direct Detection								
HgCdTe	Judson	J15D12-M204-S025U-60	0.025 mm dia.	0.15 μs	1.1 MHz	77	5×10^{10}	8.1×10^2
HgCdTe	Judson	J15D5-M204-S01M-60	1 mm dia.	5 μs	32 kHz	77	8×10^{10}	2.0×10^2
HgCdZnTe	Boston Elec.	PDI-2TE-5	1 mm ²	20 ns	8.0 MHz	230	7×10^{10}	4.0×10^3
InSb	Judson	J10D-M204-R01M-60	1 mm dia.	10 μs	16 kHz	77	7×10^{10}	1.6×10^2

Acknowledgements

This research was supported by Army SBIR grant DAAD13-03-P-0082.

References

1. Boston Electronics Model PDI-2TE-5.
2. J. E. Midwinter, Appl. Phys. Lett. **12**, 68 (1968).
3. E. A. Watson and G. M. Morris, J. Appl. Phys. **67**, 6075 (1990).
4. C. R. Brewer, P. E. Powers, S. M. Kirkpatrick, E. A. Watson, Appl. Opt. **41**, 4411 (2002).
5. Brewer, C.D., "Image upconversion of glint returns with a multiaperture lidar receiver system," Ph.D. Thesis, The Graduate School of Engineering of the University of Dayton, August 2001.
6. J. E. Midwinter, App. Phys. Lett. **14**, 29 (1969).
7. P. E. Powers, K. A. Aniolek, T. J. Kulp, B. A. Richmann, and S. E. Bisson, Opt. Lett. **23**, 1886 (1998).
8. M. Rahm, U. Bader, G. Anstett, J. -P. Meyn, R. Wallenstein, A. Borsutzky, Appl. Phys. B. **B75**, 47 (2002).
9. <http://www.fcsi.fujitsu.com/products/LWCharacteristicsTables/rm2.htm>.
10. SNLO nonlinear optics code available from A. V. Smith, Sandia National Laboratories, Albuquerque, NM 87185-1423.